RSC Advances

ROYAL SOCIETY OF CHEMISTRY

www.rsc.org/advances

Cite this: DOI: 10.1039/c0xx00000x

www.rsc.org/xxxxxx

ARTICLE TYPE

A direct warm-white-light $CaLa_2(MoO_4)_4$: Tb^{3+}, Sm^{3+} phosphor with tunable color tone via energy transfer for white LEDs

Wei Xie, Guixia Liu,* Xiangting Dong, Jinxian Wang and Wensheng Yu

Received (in XXX, XXX) Xth XXXXXXXXX 20XX, Accepted Xth XXXXXXXXX 20XX

DOI: 10.1039/b000000x

Series of Tb^{3+}, Sm^{3+} co-doped $CaLa_2(MoO_4)_4$ phosphors have been prepared via a solvothermal method without further sintering. The $CaLa_2(MoO_4)_4$: 1%Tb^{3+}, x%Sm^{3+} (x=0.0-5.0) phosphors were characterized by X-ray diffraction (XRD), field-emission scanning electron microscope (FE-SEM) and photoluminescence (PL) spectra. Upon 277 nm excitation, the phosphors exhibit strong green emission of Tb^{3+} ions and red-orange emission of Sm^{3+} ions，the quenching concentration of Sm^{3+} is determined to be about 4%. The critical distance between Tb^{3+} and Sm^{3+} has been calculated to be about 14.3 Å and the energy transfer from Tb^{3+} to Sm^{3+} occurs through the dipole-dipole interaction. The color tone of the obtained phosphors is easily modulated from blue to cool-white, green, and ultimately to warm-white-light. Furthermore, the relationship between the value of CCT for warm-white-light and the rare earth ions (Tb^{3+}, Sm^{3+}) concentration was investigated in detail. These results reveal that this kind of phosphor is a potential candidate for White LEDs.

1 Introduction

In recent years, white light emitting diodes (w-LEDs) are hoped to be the fourth-generation lighting source because of their longer lifetime, higher energy efficiency, greater reliability, and more environmentally friendly characteristics than conventional incandescent and fluorescent lamps.[1-2] Currently, there are three different ways to achieve white light based on LEDs, as shown in Fig. 1(a-b).[3-4] At present, the commercial white LEDs are fabricated by combing a blue InGaN chip with the yellow-emitting $Y_3Al_5O_{12}$: Ce^{3+} (YAG: Ce^{3+}) phosphor. However, this combination has a high correlated color temperature (CCT=7756 K) and low color rendering index (Ra<80) due to the lack of red component, which can not meet the warm-white-light demands.[5] Warm-white-light LEDs can be achieved by utilizing a UV LED chip to excite a blend of blue, green, and red emitting phosphors. Unfortunately, the strong re-absorption of the blue light by the green and red phosphors may significantly low the conversion efficiency of the device.[6-9] Therefore, it is important to design a single-phase direct warm-white-light phosphor, which is expected to overcome the above-mentioned drawbacks. For this case, many excellent phosphors have been synthesized, such as $Ca_3Sc_2Si_3O_{12}$: Ce^{3+}, Mn^{2+},[10] $KSr_4(BO_3)_3$: Dy^{3+}, Tm^{3+}, Eu^{3+},[11] $Na_3(Y, Sc)Si_3O_9$: Eu^{2+}.[12]

Owing to the characteristic emissions $^4G_{5/2}\rightarrow{}^6H_{J/2}$ (J= 5, 7, 9) of Sm^{3+} ions are in the orange-red region, they are expected to provide red color component in phosphor.[13-14] However, Sm^{3+} ions have very weak emissions under UV excitation. Tb^{3+} ions are expected to be used as green emitters in rare earth ions doped phosphors due to the high efficiency characteristic green emissions. It is well known that Tb^{3+} ions can exhibit strong blue and green emissions by adjusting the concentration of Tb^{3+} ions and excitation wavelengths. Obviously, the characteristic emissions of Tb^{3+} and Sm^{3+} ions almost cover the whole visible region. Warm-write-light can be easily realized by varying the relative composition of Tb^{3+}/Sm^{3+} and excitation wavelengths in single-phase host. Furthermore, the $^5D_3$ and $^5D_4$ emission bands of Tb^{3+} have a good overlap with the excitation bands of Sm^{3+}. It is expected that Tb^{3+} ions could transfer energy to Sm^{3+} ions, which contributes to realizing warm-write-light. In previous researches, it was reported that energy transfer played an important role in the luminescence properties of the phosphors[15]. It can not only increase the PL intensities of the phosphor, but also tune the emission color by changing the concentrations of the sensitizer and activator. Some research work has been done to develop the single-phase phosphors based on the process of energy transfer from Tb^{3+} to Sm^{3+}, such as in the host of $NaGd(WO_4)_2$,[16] $NaGdF_4$,[17] $BaCeF_5$,[18] and $Ca_2Gd_8Si_6O_{26}$.[19]

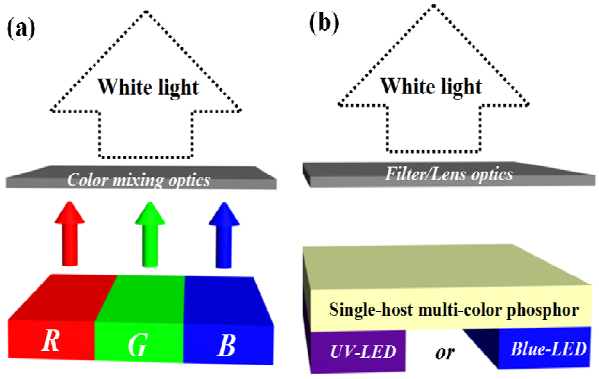

Fig. 1 Three ways of yielding white-light mechanism

As a large class of inorganic functional materials, molybdates have attracted great interest due to their wide use in catalysts, laser, and luminescence materials.[20-24] Recently, the research has focused on the double rare earth molydbates $ARE(MoO_4)_2$(A=Li, Na and K, RE= rare earth cation), which share the sheelite-like ($CaWO_4$) isostructure, owing to their broad and intense absorption band in the near-UV region, excellent thermal and hydrolytic stability, they can be widely used in white light-emitting diodes (White LEDs).[25-28] However, only few researches have done on the synthesis of rare-earth molydbates with the structure of $ARE_2(MoO_4)_4$(A=alkaline earth, RE= rare earth cation).[29-31] More importantly, there has been no reports on Tb^{3+}, Sm^{3+} co-doped in $CaLa_2(MoO_4)_4$ host up to now.

In this work, we report on the synthesis, structure, luminescence properties and energy transfer of a series of molydbate-type phosphor, $CaLa_2(MoO_4)_4$: Tb^{3+}, Sm^{3+}, which can serve as a single-phase warm-white-light phosphor based on the UV-LEDs. The emission color of the obtained phosphors is easily modulated by changing the Sm^{3+} contents. The efficient energy transfer and critical distance between Tb^{3+} and Sm^{3+} were calculated. In addition, we have also investigated the relationship between the values of CCT and the rare-earth ions (Tb^{3+}, Sm^{3+}) concentration in detail.

2 Experimental section

2.1 Materials

Aqueous solutions of $La(NO_3)_3$, $Tb(NO_3)_3$, $Sm(NO_3)_3$ and $Ca(NO_3)_3$ were obtained by dissolving the rare earth oxides La_2O_3, Tb_4O_7, Sm_2O_3, and CaO in dilute HNO_3 solution (15 mol/L) under heating with agitation in ambient atmosphere. All the other chemicals were of analytic grade and used as received without further purification.

2.2 Preparation

A series of rare earth ions-doped $CaLa_2(MoO_4)_4$ phosphors were synthesized by a facile solvothermal process without further sintering treatment. For the synthesis of $CaLa_2(MoO_4)_4$: 1%Tb^{3+}, 1%Sm^{3+} phosphor, 1.0 mmol of $RE(NO_3)_3$ (including 0.98 mmol $La(NO_3)_3$, 0.01 mmol $Tb(NO_3)_3$, 0.01 mmol $Sm(NO_3)_3$) and 0.5 mmol $Ca(NO_3)_2$ were added into 100 mL flask. After vigorous stirring for 20 min, 2.0 mmol of $Na_2MoO_4{\cdot}2H_2O$, 8.8 mL H_2O and 20 ml CH_3CH_2OH (according to the molar ratio of H_2O: CH_3CH_2OH = 1:1) was slowly added into the above solution. After additional agitation for 30 min, the as-obtained white mixing solution was transferred to a 50 mL Teflon bottle (filled up to 80% of its total volume) held in a stainless steel autoclave, and then heated at 180 °C for 20 h. Finally, as the autoclave was naturally cooled to room temperature, the precipitates were separated by centrifugation at 9000 r/min for 3 min, washed with deionized water and ethanol in sequence each three times, and then dried in oven at 60 °C for 12 h. The other samples were prepared in a similar procedure except for the doping appreciate content of rare earth ions.

2.3 Characterization

X-ray diffraction (XRD) was performed with a Rigaku D/max-RA X-ray diffractometer with Cu Kα radiation (λ= 0.15406 nm) and Ni filter, operating at a scanning speed of 10° min^{-1} in the 2θ range from 10 to 90°, 20 mA, 30 kV. The morphology of the samples was observed by field emission scanning electron microscope (FESEM) using a FEI XL-30 instrument. The excitation and emission spectra, and the luminescence decay curves of samples were measured using a HITACHI F-7000 Fluorescence Spectrophotometer equipped with a 150 W Xe lamp as the excitation source, operating at 700 V, scanning at 1200 nm/min. Both of the excitation and emission slits were set at 2.5 nm. All of the measurements were performed at room temperature.

3 Results and discussion

3.1 Phase identification and morphology

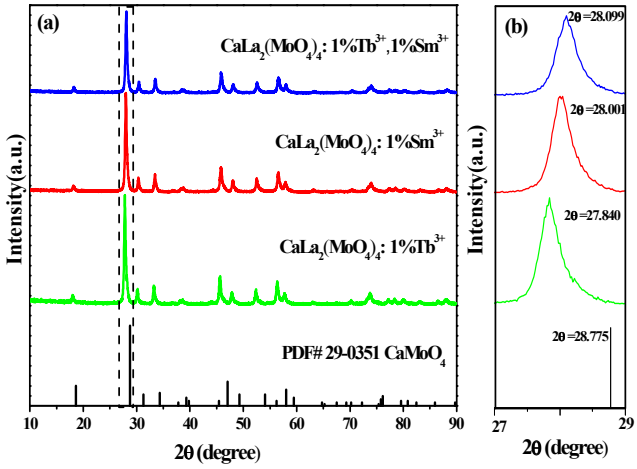

Fig. 2(a) XRD patterns of $CaLa_2(MoO_4)_4$: 1%Tb^{3+}, $CaLa_2(MoO_4)_4$: 1%Sm^{3+}, $CaLa_2(MoO_4)_4$: 1%Tb^{3+}, 1%Sm^{3+}.The standard pattern of $CaMoO_4$ (PDF#29-0351) is presented at the bottom for comparison. (b) Magnified XRD patterns in the 2θ region between 27 and 29 degree for the $CaLa_2(MoO_4)_4$: 1%Tb^{3+}, $CaLa_2(MoO_4)_4$: 1%Sm^{3+}, $CaLa_2(MoO_4)_4$: 1%Tb^{3+}, 1%Sm^{3+} phosphors.

Fig. 2a shows the XRD patterns of $CaLa_2(MoO_4)_4$: Tb^{3+}, Sm^{3+}. It is noted that all diffraction peaks of the samples are found to be well coincident with the standard $CaMoO_4$ (PDF#29-0351). The strong and sharp diffraction peaks indicate that the as-synthesized samples at low temperatures are still highly crystalline. It is also observed that the entire diffraction profiles shift to the lower angle, as depicted in Fig. 2b, owing to the larger ionic radius of La^{3+} (1.16 Å) compared with that of Ca^{2+} (1.12 Å)[32]. The diffraction profiles shift towards to the higher degree from $CaLa_2(MoO_4)_4$:1%Tb^{3+}, $CaLa_2(MoO_4)_4$: 1%Sm^{3+} to $CaLa_2(MoO_4)_4$: 1%Tb^{3+}, 1%Sm^{3+}, which can be assigned to the ionic radius for the Tb^{3+} ions (1.04 Å) and the Sm^{3+} ions (1.079 Å) are smaller than La^{3+} ions (1.16 Å).[32] In view of the ionic radius and valence state, the Tb^{3+} and Sm^{3+} ions preferentially substitute the La^{3+} ions in the $CaLa_2(MoO_4)_4$ crystal. In other words, the rare-earth ions have been effectively built into the host.

The morphology and size of the phosphors are important for their application in coatings on lighting devices.[33] Fig. 3 shows the FESEM images of $CaLa_2(MoO_4)_4$: 1.0%Tb^{3+}, 1.0%Sm^{3+} phosphor at different magnification, it is noted that the obtained phosphors take on a micro-sphere morphology with the diameter in the range of 0.2-0.8 μm and the average diameter is 0.437 μm,

seen from the particle size histogram in the inset of Fig. 3b. The result can meet the requirement of commercial White LEDs phosphors.

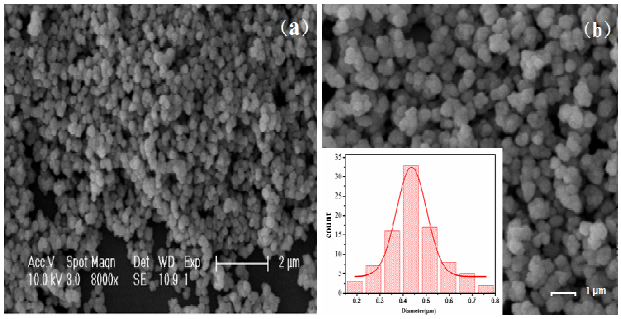

Fig. 3 FESEM images (a, b) of $CaLa_2(MoO_4)_4$: 1.0% Tb^{3+}, 1.0% Sm^{3+} phosphor. (Inset of b is the particle size histogram)

3.2 Photoluminescence properties

Fig. 4 illustrates the PLE and PL spectra for $CaLa_2(MoO_4)_4$: 1%Tb^{3+} (a) and $CaLa_2(MoO_4)_4$: 1%Tb^{3+}, 1%Sm^{3+} (b) phosphors. As seen from Fig. 4a, we have observed that the excitation spectrum of $CaLa_2(MoO_4)_4$: 1%Tb^{3+} (monitored at 545 nm) exhibits a strong excitation band from 200 to 350 nm with a maximum at 277 nm and two weak absorption peaks at 369 and 377 nm, which are assigned to the charge transfer (CTB) transition within Mo^{6+}-O^{2-} and the transitions of Tb^{3+} ions from the ground level $^7F_6$ to the $^5G_6$ and $^5D_3$ excited levels, respectively. Upon 277 nm excitation, $CaLa_2(MoO_4)_4$: 1%Tb^{3+} phosphor emits a series of luminescent peaks located at 490, 545, 586, 620 nm, which originate from the $^5D_4 \rightarrow {}^7F_J$ (J=6, 5, 4, 3) transitions of Tb^{3+}. Meanwhile, it is clearly seen that two strong green emissions (490 and 545 nm) and weak yellow and red emissions (586 and 620 nm), which could be used for obtaining excellent and abundant tunable color emissions. As seen from Fig. 4(b), the PLE spectrum of $CaLa_2(MoO_4)_4$: 1%Tb^{3+}, 1%Sm^{3+} illustrates some absorption peaks corresponding to the characteristic transitions of Tb^{3+} (369 and 377 nm) and Sm^{3+} (405 nm) when monitored by the emission of Sm^{3+} ions (564 nm), demonstrating the existence of energy transfer from the Tb^{3+} to Sm^{3+} ions in the $CaLa_2(MoO_4)_4$ host. In addition, the $CaLa_2(MoO_4)_4$: 1%Tb^{3+}, 1%Sm^{3+} presents a weaker CTB monitored at 564 nm than that monitored at 545 nm, suggesting that the energy transfer from CTB to Tb^{3+} is more efficient than that from CTB to Sm^{3+}.[34] Upon 277 nm excitation, the $CaLa_2(MoO_4)_4$: 1%Tb^{3+}, 1%Sm^{3+} phosphor exhibits the characteristic emissions of $^5D_4 \rightarrow {}^7F_J$ (J=6, 5, 4, 3) transitions of Tb^{3+} ions and $^4G_{2/5} \rightarrow {}^6H_J$ (J=5/2, 7/2, 9/2) transitions of Sm^{3+} ions, corresponding to 490, 545, 586, 625 nm, transitions for Tb^{3+} ions and 564, 594, 646 nm, transitions for Sm^{3+} ions, respectively. The emission spectrum nearly covers the entire visible region. Therefore, warm-white-light can be generated by combining the emissions of Tb^{3+} ions and orange-red emissions of Sm^{3+} ions in a single host by changing the Tb^{3+} and Sm^{3+} content via the process of energy transfer.

In order to verify the energy transfer from Tb^{3+} to Sm^{3+}, Fig. 5 presents the spectral overlap between the PL spectrum of $CaLa_2(MoO_4)_4$: 1%Tb^{3+} (dash line) and the PLE spectrum of $CaLa_2(MoO_4)_4$: 1%Sm^{3+} (solid line). The solid line is the f-f transitions of Sm^{3+} in the longer wavelength region at 405, 416, 444, 465 and 483 nm corresponding to the electronic transitions of Sm^{3+} ions from the ground level $^6H_{5/2}$ to the $^4K_{11/2}$, $^6P_{5/2}$, $^4G_{9/2}$, $^4F_{5/2}$ and $^4I_{11/2}$ excited levels, respectively.

Furthermore, we can find that the strongest peak is located at 405 nm, which is suitable to be used for near-UV LED excited phosphors.[16] The dash line is the $^5D_3$ and $^5D_4$ emissions of Tb^{3+}, we also observed the strong peak at 490 nm. Due to the d-d forbidden transitions of Sm^{3+}, their excitation transitions are difficult to excite and the emission intensity is very weak. Therefore, the energy transfer was expected to occur from Tb^{3+} to Sm^{3+}. Based on the effective spectral overlap from Fig. 5, it is found that the $^5D_3$ and $^5D_4$ emission bands of Tb^{3+} overlap the excitation bands of Sm^{3+}. Based on the above discussion, the significant energy transfer from Tb^{3+} to Sm^{3+} is expected to occur in $CaLa_2(MoO_4)_4$ system.

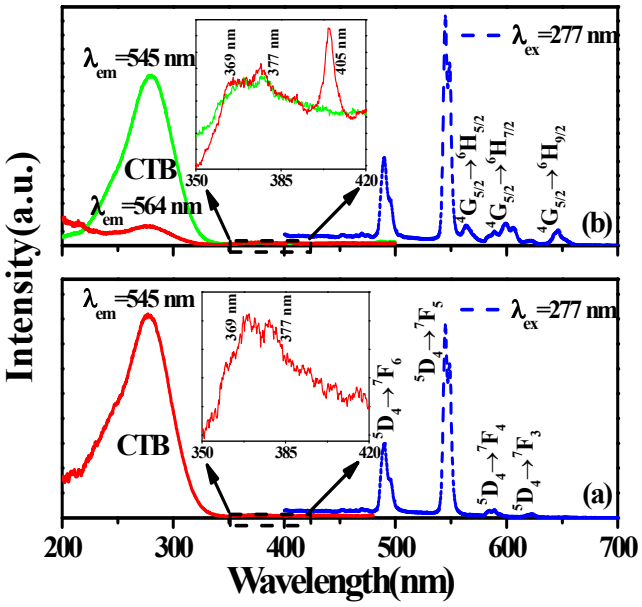

Fig. 4 Photoluminescence excitation (PLE) and Photoluminescence (PL) spectra for $CaLa_2(MoO_4)_4$: 1%Tb^{3+} (a) and $CaLa_2(MoO_4)_4$: 1%Tb^{3+}, 1%Sm^{3+} (b) phosphors.

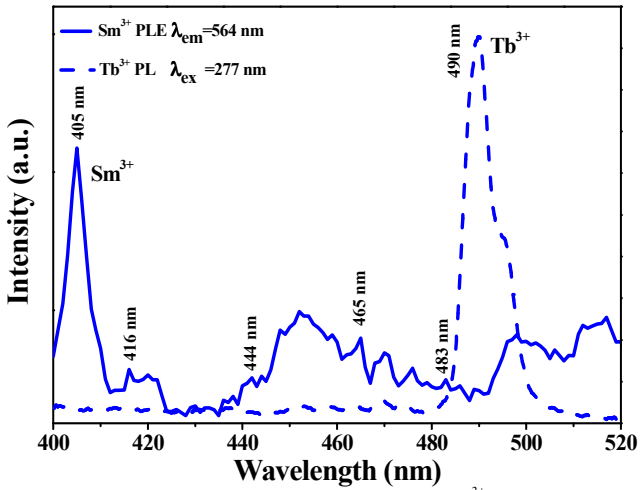

Fig. 5 The PL emission spectrum of $CaLa_2(MoO_4)_4$: 1%Tb^{3+} (dash line) and the PLE spectrum of $CaLa_2(MoO_4)_4$: 1%Sm^{3+} (solid line).

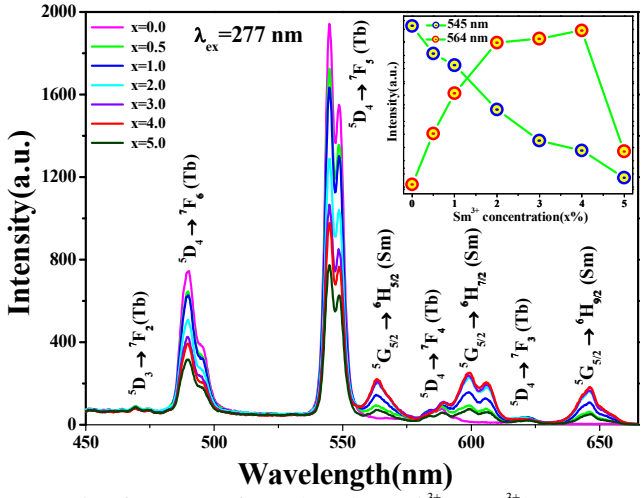

Fig. 6 Series of PL spectra of $CaLa_2(MoO_4)_4$: 1%Tb^{3+}, x%Sm^{3+}(x = 0.0，0.5, 1.0, 2.0, 3.0, 4.0, 5.0) under UV excitation (λ_{ex} = 277 nm). The inset shows the dependence of Tb^{3+} and Sm^{3+} emission intensity on the Sm^{3+} concentrations.

A series of $CaLa_2(MoO_4)_4$: 1%Tb^{3+}, x%Sm^{3+}(x=0.0, 0.5, 1.0, 2.0, 3.0, 4.0, 5.0) samples have been prepared to further study the energy transfer phenomenon from Tb^{3+} to Sm^{3+}. Fig. 6 illustrates the PL emission spectra of the Tb^{3+}, Sm^{3+} co-doped $CaLa_2(MoO_4)_4$ phosphors with different Sm^{3+} doped concentrations. Upon 277 nm excitation, the PL spectra consist of the typical green emissions of Tb^{3+} and the typical orange-red emissions of Sm^{3+}. Furthermore, we find that the PL intensities of $^5D_4 \rightarrow {}^7F_6$ (490 nm) and $^5D_4 \rightarrow {}^7F_5$ (545 nm) transitions for Tb^{3+} decrease monotonically with an increase in doping Sm^{3+} concentration. Meanwhile, the emissions of $^4G_{5/2} \rightarrow {}^6H_{5/2}$ (564 nm), $^4G_{5/2} \rightarrow {}^6H_{7/2}$ (594 nm) and $^4G_{5/2} \rightarrow {}^6H_{9/2}$ (648 nm) of Sm^{3+} increase gradually until the Sm^{3+} concentration is above 4% and then decrease for the concentration quenching, which can be easily observed from the inset of Fig. 6. These results give us another evidence to validate energy transfer from Tb^{3+} to Sm^{3+}. In addition, as shown in Fig. 6, one can see that the emission peak of the Sm^{3+} shifts toward short wavelength with gradually increasing the doping concentration of Sm^{3+}, which originates from the change of crystal field strength.[8, 35]

Generally speaking, the critical distance (R_C) of energy transfer is calculated by using the concentration quenching method estimated by the following formula suggested by Blasse:[36-37]

$$R_c = 2\times[3V/(4\pi x_c Z)]^{1/3} \quad (1)$$

where V is the volume of the unit cell, Z is the number of host cations in the unit cell. For $CaLa_2(MoO_4)_4$ host lattice, Z=4, V=312.2 Å^3. x_C is the total concentration of the sensitizer ions of Tb^{3+} and the activator ions of Sm^{3+} at which the luminescence intensity of Tb^{3+} is half of that the sample in the absence of Sm^{3+}. According to the inset of Fig. 6, x_C is 0.051. From the above formula, the critical distance (R_C) of the energy transfer is estimated to be about 14.3 Å. The energy transfer process can be defined as two interaction models: multipolar and exchange interaction. While the critical distance in exchange interaction model should be less than 4 Å.[38] The critical distance analysis indicates that the energy transfer from Tb^{3+} to Sm^{3+} has occurred via multipolar interaction.

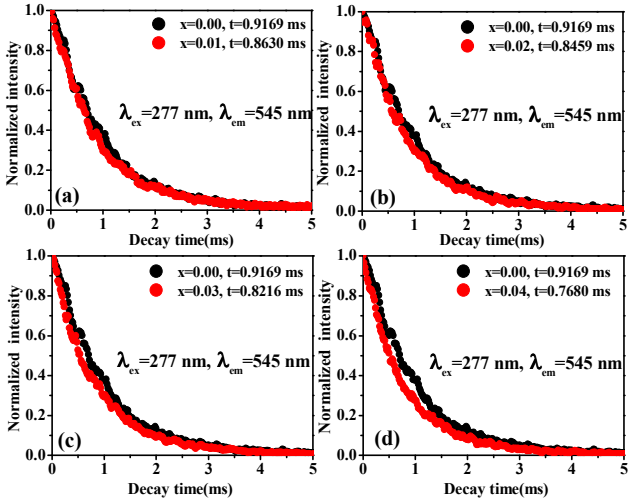

Fig. 7 Decay curves for the luminescence of Tb^{3+} ions in $CaLa_2(MoO_4)_4$:1%Tb^{3+}, x%Sm^{3+} (x=1.0, 2.0, 3.0, 4.0) phosphors displayed on a normalized intensity (a-d) (excited at 277 nm, monitored at 545 nm).

In order to well understand the mechanism of the energy transfer process, the fluorescent decay curves of $CaLa_2(MoO_4)_4$:1%Tb^{3+}, x%Sm^{3+}(x=1.0, 2.0, 3.0, 4.0) samples were measured by monitoring the emission of Tb^{3+} at 545 nm. As shown from Fig. 7(a)-(d), it is easily found that all the decay curves of Tb^{3+} can be fitted to a single exponential function as:

$$I = I_0 + A\, e^{-t/\tau} \quad (2)$$

where I represents the intensity at any time, I_0 is the intensity at t = 0, and τ is the decay lifetime. The lifetime values of Tb^{3+} are 0.9169, 0.8630, 0.8459, 0.8216, 0.7680 ms for $CaLa_2(MoO_4)_4$: 1%Tb^{3+}, x%Sm^{3+}(x=1.0, 2.0, 3.0, 4.0), respectively. It can be found that the decay lifetimes of the Tb^{3+} decrease monotonically with an increase of Sm^{3+} concentration, which is strong evidence for the energy transfer between Tb^{3+} and Sm^{3+}.

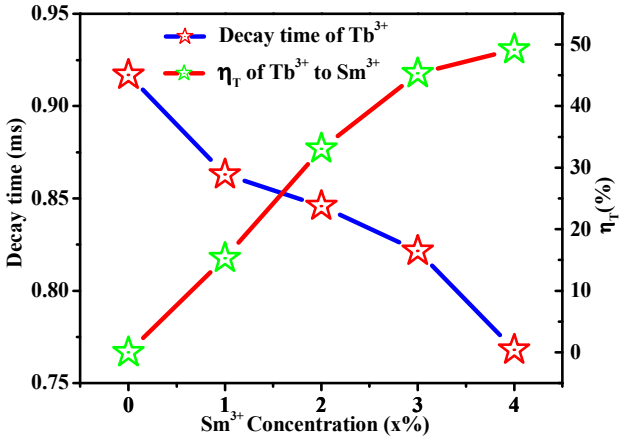

Fig. 8 Dependence of the decay time of the Tb^{3+} and energy transfer efficiency η_T on doped Sm^{3+} concentration in $CaLa_2(MoO_4)_4$: 1%Tb^{3+}, x%Sm^{3+} (x= 0.0, 1.0, 2.0, 3.0, 4.0) phosphors.

Fig. 8 shows the decay time of the Tb^{3+} and the energy transfer efficiency from Tb^{3+} to Sm^{3+} as a function of Sm^{3+} doping concentration in host. The energy transfer efficiency η_T from the sensitizer to the activator can be calculated by the following equation: [39]

$$\eta_T = 1 - I_S/I_{S0} \quad (3)$$

where I_{S0} and I_S are the luminescence intensity of a sensitizer in the absence and presence of an activator, respectively. For the $CaLa_2(MoO_4)_4$:Tb^{3+}, Sm^{3+} phosphor, Tb^{3+} is the sensitizer and Sm^{3+} is the activator. As shown from Fig. 8, it can be seen that the fluorescence lifetime value of Tb^{3+} (τ) is straight reduced with increasing the Sm^{3+} content while the energy transfer efficiency (η_T) is not in the same trend which increases monotonically. In detail, the values of η_T were calculated to be 0.00, 15.52%, 33.07%, 45.33% and 49.20% for $CaLa_2(MoO_4)_4$: 1%Tb^{3+}, x%Sm^{3+}(x=0.0, 1.0, 2.0, 3.0, 4.0), respectively. These above results reveal that the energy migration from Tb^{3+} to Sm^{3+} is valid.

Based on the discussion above, it is easy for us to draw the conclusion that the energy transfer mechanism from the Tb^{3+} to Sm^{3+} ions is a multipolar interaction. According to Dexter's energy transfer formula of exchange and multipolar interaction, the following relation can be given as: [40]

$$I_{S0}/I_S \propto C^{n/3} \quad (4)$$

where I_{S0} and I_S are the luminescence intensity of Tb^{3+} ions in the absence and presence of Sm^{3+} ions, respectively. C is the sum of Tb^{3+} ions and Sm^{3+} ions concentration, and n=6, 8, and 10, corresponds to dipole-dipole, dipole-quadrupole, and quadrupole-quadrupole interactions, respectively. Fig. 9 presents the relationships between (I_{S0}/I_S) versus $C^{n/3}$, and the best linear relationship is obtained when n=6. This result clearly demonstrates that the energy transfer mechanism from the Tb^{3+} to Sm^{3+} ions is a dipole-dipole interaction.

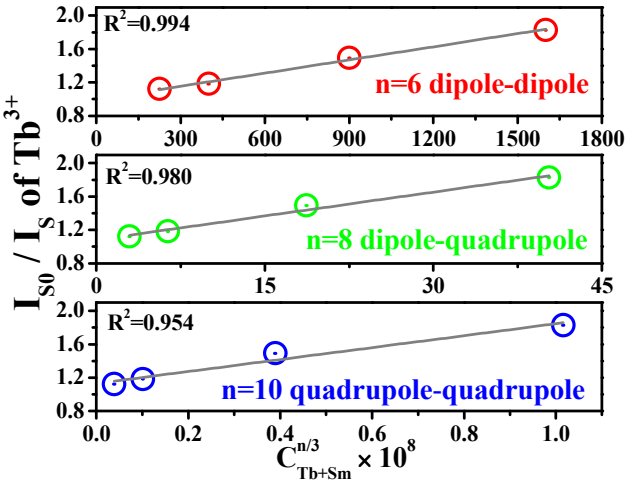

Fig. 9 The dependence I_{S0}/I_S of Tb^{3+} in $CaLa_2(MoO_4)_4$: 1%Tb^{3+}, x%Sm^{3+} (x=0.5, 1.0, 2.0, 3.0) phosphors.

To further research the dipole-dipole interaction, the energy transfer probability P_{SA} from a sensitizer to an accepter is given by the following equation: [41]

$$P_{SA}=(1/\tau) - (1/\tau_0) \quad (5)$$

where τ and τ_0 are the decay lifetimes of Tb^{3+} presence and absence the Sm^{3+} ions. On the basis of above equation, the energy transfer probabilities from Tb^{3+} to Sm^{3+} are calculated to be 0.06812, 0.09154, 0.12651 and 0.21145 for the $CaLa_2(MoO_4)_4$: 1%Tb^{3+}, x%Sm^{3+}(x=0.0, 1.0, 2.0, 3.0, 4.0), respectively. This result demonstrates that with an increase in Sm^{3+} concentrations, the energy transfer probability from Tb^{3+} to Sm^{3+} increases.

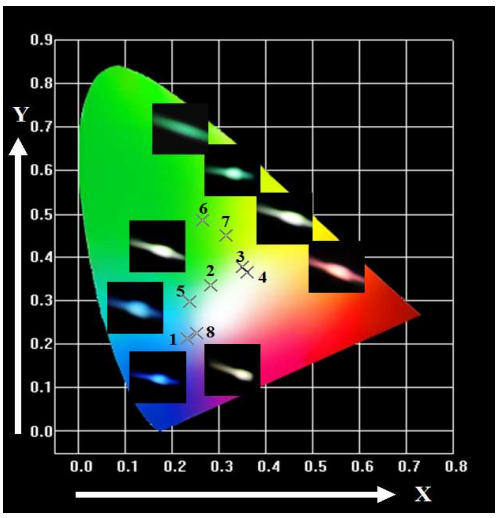

Fig. 10 CIE chromaticity diagram of the selected $CaLa_2(MoO_4)_4$: Tb^{3+}, Sm^{3+} phosphors under 277 nm (3, 4, 5, 6, 7), 365 nm (1), 370 nm (8) and 405 nm (2) excitation. The corresponding images under corresponding excitation wavelengths.

The Commission International de I'Eclairage(CIE) chromaticity coordinates and the correlated color temperature(CCT) for the single-phase $CaLa_2(MoO_4)_4$: Tb^{3+}, Sm^{3+} phosphors under different excitation wavelengths (277, 365, 370, 405 nm) are summarized in Table1. As shown in Fig. 10, it can be observed that the color hue of the obtained phosphors can be easily modulated from blue (point 1, 5) to cool-white (point 2, 8), green (point 6, 7), and ultimately to warm-white (point 3, 4). Moreover, the points 3 and 4 show lower CCT values (4932, 4533 K), which meet the commercial warm-white-light requirement. All the above results reveal that the $CaLa_2(MoO_4)_4$: Tb^{3+}, Sm^{3+} phosphors can be used as a potential multicolor phosphor for W-LED application.

For the application of White LEDs, the correlated color temperature of the phosphor is one of the important factors. As we all known, the correlated color temperature for a warm-white-light should be less than 5000 K, which is popular in solid state lighting.[11] Fig. 11 presents the relationship of the correlated color temperature for $CaLa_2(MoO_4)_4$: Tb^{3+}, Sm^{3+} phosphors with different Sm^{3+} and Tb^{3+} doping concentrations. Fig. 11(a) shows that the values of correlated color temperature are calculated to be 4932, 4630, 4164, 4534 K for the $CaLa_2(MoO_4)_4$: 0.1%Tb^{3+}, x%Sm^{3+} (x=5.0, 6.0, 7.0, 8.0), respectively. With an increase in Sm^{3+} concentration, we can find that the CCT decreases gradually until the Sm^{3+} concentration arrives at 7%, this phenomenon

Table1 Comparison of the CIE chromaticity coordinates(x, y) and correlated color temperature for $CaLa_2(MoO_4)_4$: Tb^{3+}, Sm^{3+} phosphors

Point	Sample	Excitation(nm)	CIE (x, y)	CCT(K)
1	0.05%Tb^{3+}, 5%Sm^{3+}	365	(0.232, 0.212)	108458
2	0.05%Tb^{3+}, 5%Sm^{3+}	405	(0.282, 0.334)	8255
3	0.1%Tb^{3+}, 5%Sm^{3+}	277	(0.349, 0.377)	4932
4	0.1%Tb^{3+}, 6%Sm^{3+}	277	(0.360, 0.366)	4533
5	0.05%Tb^{3+}, 5%Sm^{3+}	277	(0.238, 0.298)	14047
6	1%Tb^{3+}, 0.5%Sm^{3+}	277	(0.266, 0.485)	7208
7	1%Tb^{3+}, 4%Sm^{3+}	277	(0.315, 0.449)	5973
8	1%Tb^{3+}, 4%Sm^{3+}	370	(0.252, 0.226)	36872

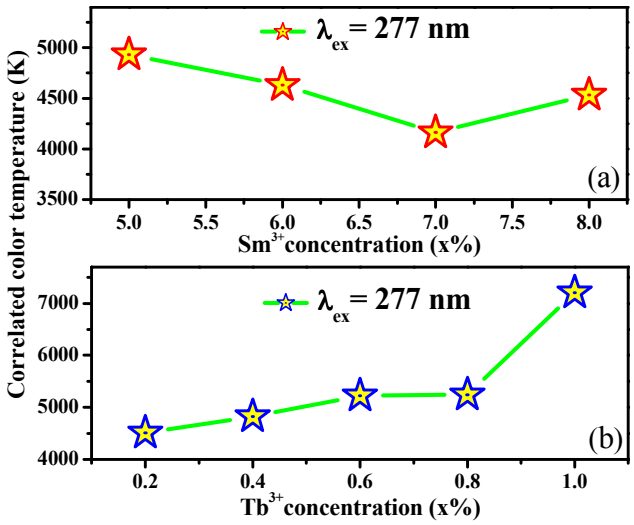

Fig. 11 Correlated color temperature of the $CaLa_2(MoO_4)_4$: 0.1%Tb^{3+}, x%Sm^{3+} (x=5.0, 6.0, 7.0, 8.0)(a) and $CaLa_2(MoO_4)_4$: x%Tb^{3+}, 5%Sm^{3+} (x=0.2, 0.4, 0.6, 0.8, 1.0)(b) phosphors under 277 nm excitation.

should result from the Sm^{3+} concentration quenching. From Fig. 11(b), the values of correlated color temperature are calculated to be 4510, 4823, 5225, 5242, 7207 K for the $CaLa_2(MoO_4)_4$: x%Tb^{3+}, 5%Sm^{3+} (x=0.2, 0.4, 0.6, 0.8, 1.0), respectively. Obviously, the values of CCT gradually increase as the concentration of Tb^{3+} increases. According to the above results, the values of CCT are closely related the Tb^{3+} and Sm^{3+} concentration, which have guiding significance for the application of commercial White LEDs.

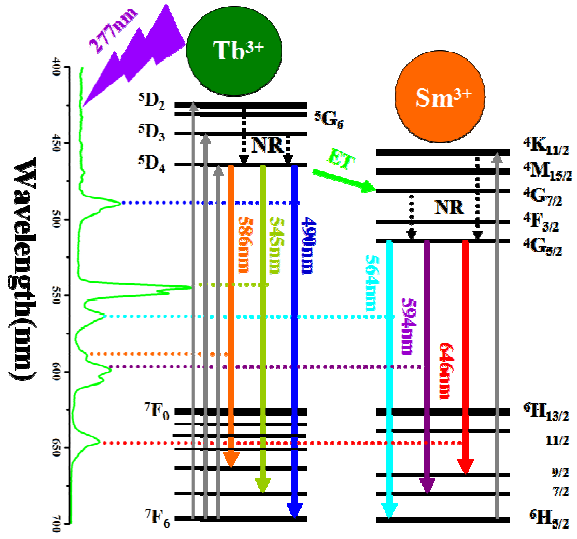

Fig. 12 Schematic energy-level diagram showing the excitation and emission mechanisms of $CaLa_2(MoO_4)_4$: Tb^{3+}, Sm^{3+} phosphors (ET: energy transfer; NR: nonradiative).

In order to further describing the excitation and emission mechanisms in detail, we depict the energy-level diagram of Tb^{3+} and Sm^{3+} co-doped $CaLa_2(MoO_4)_4$, shown in Fig. 12. It can be found that the electrons can absorb energies of photons from 277 nm UV light, when the electrons return to lower energy-level via multi-color emission and energy transfer from Tb^{3+} to Sm^{3+} ions, and some energy is lost by cross relaxation.

4 Conclusions

In summary, a series of color tunable phosphors from blue to warm-white-light were successfully realized with Tb^{3+} and Sm^{3+} co-doped in a $CaLa_2(MoO_4)_4$ host. Upon 277 nm excitation, the phosphors show the intense green emissions of Tb^{3+} and the typical orange-red emissions of Sm^{3+}. As for $CaLa_2(MoO_4)_4$: 1%Tb^{3+}, x%Sm^{3+}, the quenching concentration of Sm^{3+} was about x=4.0. The photoluminescence and fluorescence decay times demonstrate that the energy transfer from Tb^{3+} to Sm^{3+} is expected. The critical distance for Tb^{3+} to Sm^{3+} has been calculated to be 14.3 Å by the basis of Dexter theory. The analysis indicates that the dipole-dipole interaction should be responsible for this energy transfer. The CIE coordinates show that the color hue can be tunable from blue to cool-white, green, and ultimately to warm-white-light. The CCT of warm-white-light emission required were obtained, which closely related to the Tb^{3+} and Sm^{3+} concentration. The results indicate that the as-synthesized phosphors have huge potential to be a single host warm-white-light phosphor for White LEDs.

Acknowledgements

This work was supported by the National Natural Science Foundation of P.R. China (NSFC) (Grant No. **51072026**, **50972020**) and the Development of Science and Technology Plan Projects of Jilin Province (Grant No. **20130206002GX**).

Notes and references

Key Laboratory of Applied Chemistry and Nanotechnology at Universities of Jilin Province, Changchun University of Science and Technology, Changchun, China. Fax: +86-431-85383815; Tel: +86-431-85582574; E-mail: liuguixia22@163.com

1. E. F. Schubert and J. K. Kim, *Science*, 2005, **308**, 1274-1278.
2. Y. Narukawa, J. Narita, T. Sakamoto, T. Yamada, H. Narimatsu, M. Sano and T. Mukai, *Phys. Status Solidi A*, 2007, **204**, 2087-2093.
3. S.Ye, F. Xiao, Y. X. Pan, Y. Y. Ma and Q. Y. Zhang, *Mater. Sci. Eng., R,* 2010, **71**, 1-34.
4. J. S. Hou, W. Z. Jiang, Y. Z. Fang and F. Q. Huang, *J. Mater. Chem. C*, **1**, 5892-5898.
5. V. Bachmann, C. Ronda and A. Meijerink, *Chem. Mater.*, 2009, **21**, 2077-2084.
6. T. S. Chan, R. S. Liu and I. Baginskiy, *Chem. Mater.*, 2008, **20**, 1215-1217.
7. C. F. Guo, L. Luan, F. G. Shi and X. Ding, *J. Electrochem. Soc.,* 2009, **156**, J125.
8. R. J. Xie, N. Hirosaki, M. Mitomo, K. Sakuma and N. Kimura, *Appl. Phys. Lett.*, 2006, **89**, 241103.
9. Z. G. Xia, X. M. Wang, Y. X. Wang, L. B. Liao and X. P. Jing, *Inorg.Chem.*, 2011, **50**, 10134-10142.
10. Y. F. Liu, X. Zhang, Z. D. Hao, Y. S. Luo, X. J. Wang and J. H. Zhang, *J. Mater. Chem.*, 2011, **21**, 16379-16384.
11. L. Wu, Y. Zhang, M. Y. Gui, P. Z. Lu, L. X. Zhao, S. Tian, Y. F. Kong and J. J. Xu, *J. Mater. Chem.*, 2012, **22**, 6463-6470.
12. Z. G. Xia and Z. Y. Mao, *J. Mater. Chem. C*, 2013, **1**, 5917-5924.
13. R. Satheesh Kumar, V. Ponnusamy and M. T. Jose, *Luminescence*, 2013, **29**, 649-656.
14. C. Y. Jia, W. Lü, N. Guo, W. Lv, Q. Zhao and H. P. You, *Chem. Commun.,* 2013, **49**, 2664-2666.
15. P. P. Dai, X. T. Zhang, L. L. Bian, S. Lu, Y. C. Liu and X. J. Wang, *J. Mater. Chem. C*, 2013, **1**, 4570-4576.
16. Y. Liu, G. X. Liu, X. T. Dong, J. X. Wang and W. S. Yu, *RSC Advances.*, 2014, **4**, 45389-45396.
17. H. X. Guan, G. X. Liu, X. T. Dong, J. X. Wang and W. S. Yu, *Dalton*

Trans., 2014, **43**, 10801–10808.
18. T. Sheng, Z. Fu, X. Wang, S. Zhou, S. Zhang and Z. Dai, *J. Phys. Chem. C*, 2012, **116**, 19597-19603.
19. G. S. R. Raju, J. Y. Park, H. C. Jung, E. Pavitra, B. K. Moon, J. H. Jeong and J. H. Kim, *J. Mater. Chem.*, 2011, **21**, 6136-6139.
20. C. Mazzocchia, C. Aboumrad, C. Diagne, E. Tempesti, J. M. Herrmann and G. Thomas, *Catal. Lett.*, 1991, **10**, 181.
21. D. Spassky, S. Ivanov, I. Kitaeva, V. Kolobanov,V. Mikhailin, L. Ivleva and I. Voronina, *Phys. Status Solidi C*, 2005, **2**, 65-68.
22. H. Barry, F. Moore and D. Robitaille, *US Pat,* 3 726 694, 1973.
23. S. S. Kim, S. Ogura, H. Ikuta, Y. Uchimoto and M. Wakihara, *Chem. Lett.*, 2001, **30**, 760-761.
24. R. Sundaram and K. S. Nagaraja, *Sens. Actuators, B*, 2004, **101**, 353-360.
25. T. Wu, Y. F. Liu, Y. N. Lu, L. Wei, H. Gao and H. Chen, *CrystEngComm*, 2013, **15**, 2761–2768.
26. V. A. Morozov, B. I. Lazoryak, S. Z. Shmurak, A. P. Kiselev, O. I. Lebedev, N. Gauquelin, J. Verbeeck, J. Hadermann and G. V. Tendeloo, *Chem. Mater.*, 2014, **26**, 3238-3248.
27. Y. S. Hu, W. D. Zhuang, H. Q. Ye, D. H. Wang, S. S. Zhang and X. W. Huang, *J.Alloys Compd.*, 2005, **390**, 226-229.
28. L. Xu, X. Y. Yang, H. M. Lu, C. H. Hu and W. H. Hou, *RSC Adv.*, 2014, **4**, 13502–13508.
29. V. A. Morozov, A. Bertha, K. W. Meert, S. V. Rompaey, D. Batuk, G. T. Martinez, S. V. Aert, P. F. Smet, M. V. Raskina, D. Poelman, A. M. Abakumov and J. Hadermann, *Chem. Mater.*, 2013, **25**, 4387-4395.
30. C. F. Guo, H. K. Yang and J. H. Jeong, *Luminescence,* 2010, **130**, 1390-1393.
31. J. S. Liao, D. Zhou, B. Yang, R. Q. Liu, Q. Zhang and Q. H. Zhou, *Luminescence,* 2013, **134**, 533-538.
32. R.D. Shanan, *Acta Cryst*., 1976, A32, 751-767.
33. L. Hou, S. B. Cui, Z. L. Fu, Z. J. Wu, X. H. Fu and H. Jeong, *Dalton Trans.*, 2014, **43**. 5382-5392.
34. Y. H, Zheng, Y. J. Huang, M. Yang, N. Guo, H. Qiao, Y. C. Jia and H. P. You, *J. Lumin.*,2012, **132**, 362-367.
35. G. Blasse, *J. Solid State Chem.*, 1986, **62**, 207-211.
36. G. Blasse, *Philips Res. Rep.*, 1969, **24**, 131-144.
37. C. H. Huang and T. M. Chen, *J. Phys. Chem. C*, 2011, **115**, 2349-2355.
38. B. M. Antipeuko, I. M. Bataev, V. L. Ermolaev, E. I. Lyubimov and T. A. Pricalova, *Opt. Spectrosc.*, 1970. **29**. 177-180.
39. P. I. Paulose, G. Jose, V. Thomas, N. V. Unnikrishnan and M. K. R.Warroer, *J. Phys. Chem. Solids*, 2003, **64**, 841-846.
40. D. L. Dexter and J. H. Schulman, *J. Chem. Phys.*, 1954, **21**, 836-850.
41. G. S. R. Raju, J. Y. Park, H. C. Jung, E. Pavitra, B. K. Moon, J. H. Jeong and J. H. Kim, *J. Mater. Chem.*, 2011, **21**, 6136–6139.